

Cite this: *Mol. BioSyst.*, 2017,
13, 2036

Murine cutaneous leishmaniasis investigated by MALDI mass spectrometry imaging†

Fernanda Negrão,¹ Daniele F. de O. Rocha,^a Caroline F. Jaeger,^a
Francisca J. S. Rocha,^c Marcos N. Eberlin^a and Selma Giorgio^b

Imaging mass spectrometry (IMS) is recognized as a powerful tool to investigate the spatial distribution of untargeted or targeted molecules of a wide variety of samples including tissue sections. *Leishmania* is a protozoan parasite that causes different clinical manifestations in mammalian hosts. Leishmaniasis is a major public health risk in different continents and represents one of the most important neglected diseases. Cutaneous lesions from mice experimentally infected with *Leishmania* spp. were investigated by matrix-assisted laser desorption ionization MS using the SCiLS Lab software for statistical analysis. Being applied to cutaneous leishmaniasis (CL) for the first time, MALDI-IMS was used to search for peptides and low molecular weight proteins (2–10 kDa) as candidates for potential biomarkers. Footpad sections of Balb/c mice infected with (i) *Leishmania amazonensis* or (ii) *Leishmania major* were imaged. The comparison between healthy and infected skin highlighted a set of twelve possible biomarker proteins for *L. amazonensis* and four proteins for *L. major*. Further characterization of these proteins could reveal how these proteins act in pathology progression and confirm their values as biomarkers.

Received 8th July 2017,
Accepted 27th July 2017

DOI: 10.1039/c7mb00411g

rsc.li/molecular-biosystems

Introduction

The leishmaniasis are a complex group of diseases caused by more than 20 different *Leishmania* species. These protozoan parasites are transmitted to humans by the bite of infected sandflies, and globally, there are an estimated 1.5–2 million new cases and 70 000 deaths each year, and 350 million people are at risk of infection.¹ Leishmaniasis is endemic in 88 countries and affects two million people every year. These diseases may present themselves as cutaneous, mucocutaneous or visceral forms, depending on which species is involved in the infection.² Cutaneous leishmaniasis (CL) is the most common form of the disease, and usually causes ulcers on the exposed parts of the body, such as the face, arms or legs.² The control of vectors (sandflies) and reservoirs in vector-borne diseases is difficult due to challenges of interventional programs, mainly in developing countries, where their prevalence is high.³ Current drugs against leishmaniasis lack in safety and efficacy,

and there is no vaccine against the disease.⁴ The diagnosis of CL is based on clinical features and laboratory testing with a huge variation in accuracy.⁵

In the life cycle of *Leishmania*, the promastigote form is transmitted from the sandfly to a mammalian host during a blood meal. Inside the host macrophages, the parasites differentiate into the intracellular amastigote form.^{6,7} To survive within the hostile environment of the macrophage, the parasite has various strategies to defeat the microbicidal power of the macrophage and to decrease an effective host immune response.⁸ Many studies about peptides and proteins focusing on leishmaniasis have considered a variety of aspects of parasite biology and host interactions, drug resistance mechanisms, and the identification of immunogenic proteins for vaccine development.^{9–13} These studies have improved our understanding of the pathogenesis of *Leishmania*. The events related to *Leishmania*–host cell interactions remain however poorly understood.⁹ In this study, we have focused on two etiological agents of CL aiming to unveil molecular signatures of disease progression *in situ*: (i) *L. amazonensis*, a species mainly transmitted in the Amazon region and (ii) *L. major*, transmitted in Asia and Africa.² Discovery of new proteins or peptides that could function as biomarkers while also providing information about disease progression would deepen the understanding of leishmaniasis biology, since the effective control of CL as well as other clinical forms must rely on proper diagnosis and treatment.¹⁴

Mass spectrometry (MS) is a fast, highly sensitive and selective analytical technique that can reveal the chemical

^a ThoMson Mass Spectrometry Laboratory, University of Campinas – UNICAMP, Campinas-SP, Brazil. E-mail: negraosf@gmail.com

^b Department of Animal Biology, Biology Institute, University of Campinas UNICAMP, Campinas-SP, Brazil

^c Department of Tropical Medicine, Federal University of Pernambuco – UFPE, Recife-PE, Brazil

† Electronic supplementary information (ESI) available: Histological analysis; pLSA loadings; a complete table of relevant ions; AUC information about the most relevant *m/z* interval in biological triplicates and box plots. See DOI: 10.1039/c7mb00411g

composition of a sample using low sample quantities that can complement morphological data obtained from traditional diagnostic techniques based upon microscopy inspection or immunological assays.¹⁹ MS analysis is therefore able to screen for biomarkers, and it has produced remarkable results in pharmaceutical,^{15–18} biological,^{19–22} and medical^{23,24} fields.

One of the latest developments in MS screening for biomarkers is imaging MS (IMS) using different ionization techniques such as matrix-assisted laser desorption ionization (MALDI) and desorption electrospray ionization (DESI). IMS has greatly advanced over the past years and has been demonstrated as an outstanding protocol in the analysis of histological sections of biological tissues by providing detailed information on the whole pool of molecular species distributed along a whole 2D or even 3D²⁵ surface in a particular sample.^{26,27}

IMS enables therefore the visualization of the spatial distribution of a huge variety of biomolecules in a unprocessed tissue section in a label-free manner.^{28,29} For peptides and proteins, MALDI is the most suitable ionization technique for IMS and has been used to search for biomarkers used as prognostic and/or diagnostic indicators in several tumors.^{30–34} The spatial distribution of biomolecules obtained by IMS can be compared with the results of standard protocols such as histology and immunohistochemistry (IHC).³⁵

Most of the previous studies regarding the leishmaniasis proteome evaluated proteins larger than 15 kDa.^{10,11,36} We therefore used MALDI-IMS to screen for peptides and low molecular weight (LMW) proteins within the m/z 2 to 10k range. Peptides and LMW proteins differentially expressed in the liver during visceral leishmaniasis, another clinical form of the disease, were investigated using the same ionization technique as presented.³⁷ MALDI-IMS was applied to CL lesions in mice at different disease stages aiming to compare the peptide and LMW protein profiles of healthy footpads

with footpad lesions caused by *L. amazonensis* or *L. major*. Statistical analysis was performed to highlight peptides or LMW proteins that could be related to disease progression. To the best of our knowledge, this is the first MALDI-IMS investigation of CL.

Results and discussion

Cutaneous leishmaniasis disease progression

The course of CL was first monitored by micro- and macroscopic analysis, through the histology of footpad tissue sections (Fig. 1) and measurements of footpad enlargement during infection progression using a dial caliper (Fig. S1, ESI[†]). Histological analysis confirmed the infection and added information about the progression of CL at the dermis, showing that disease progression was different for the two studied species under the same conditions. For *L. major*, at 30 days p.i., the dermis was still preserved, but defense cells were being recruited. In contrast, also at 30 days, *L. amazonensis* infection already presents signs of necrosis into the dermis.

At 60 days p.i., necrosis starts to progress in *L. major* infection, whereas the tissue for *L. amazonensis* infection was devastated due to severe necrosis and there were also signs of granulomas. After 90 days, the tissues were microscopically similar. Macroscopically, however, the clinical conditions of the footpads from mice infected with *L. amazonensis* (Fig. 1A–C) were considerably worse than the ones infected with *L. major* (Fig. 1D–F). Fig. S2 and S3 (ESI[†]) provide detailed information regarding macro- and microscopic analysis at 30 days p.i., when more differences were observed between the infections.

MALDI IMS and data processing

Raw data from MALDI IMS were loaded into SCiLS Lab software and normalized using the total ion count (TIC). A segmentation

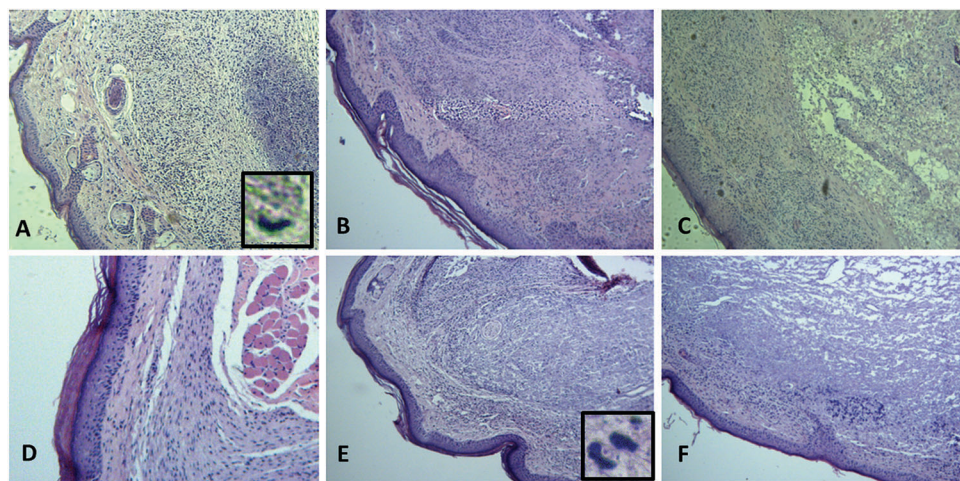


Fig. 1 Panoramic view of histological analysis of footpads at different stages (40 \times). A, B and C belong to *L. amazonensis* infection, whereas D, E and F belong to *L. major* infection. Epidermis is preserved in all stages. At 30 days p.i., the infection caused by *L. amazonensis* (A) shows signs of edema, abundant inflammatory infiltrates, infected macrophages (1000 \times) and a focus of necrosis. The dermis is still preserved. At 60 days p.i. (B), the dermis is suffering from wellspread necrosis and inflammatory cells. At 90 days p.i. (C), the dermis is severely compromised. At 30 days p.i., the infection caused by *L. major* (D) shows signs of edema. Infected macrophages are rare and necrosis is not observed. At 60 days p.i. (E) the dermis is mostly preserved, however, signs of necrosis are observed. Infected macrophages are shown in the inset (1000 \times). At 90 days p.i. (F), the dermis is severely compromised.

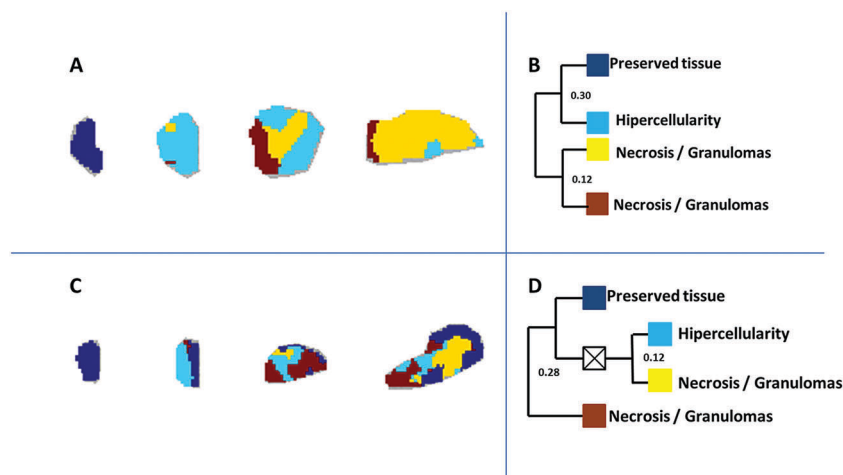


Fig. 2 Segmentation mapping results for *L. amazonensis* (A) and *L. major* (C). The figure also illustrates dendrograms (B and D) with the respective correlation distances (numbers), and the images are color assigned.

map³⁸ allowed the correlation between MALDI IMS and histological analysis. In the first trial, spectra were acquired in the m/z 2–20k range, but peak information was narrowed to the m/z 2–10k range to obtain a better resolution at this m/z range (data not shown). A spatial segmentation map^{38,39} allows regions to be clustered according to the similarities of the spectra. This approach can be considered as semi-supervised, in which a hierarchical clustering dendrogram allows the operator to explore the data interactively.⁴⁰ The results suggested four clusters (Fig. 2), whereas histological analysis showed very similar biological events for both species. Once histology was correlated with the MALDI-IMS data, the dark blue cluster corresponds to the healthy footpad, when the dermis is still preserved. The light blue cluster is related to a very intense infiltrate of defense cells. The yellow and brown clusters share two inflammatory events in common: necrosis and granulomas. Abundant infiltrates of inflammatory cells are clearly present at the first stages of infection, whereas necrosis and granulomas are dispersed at the later stages of infection. The yellow and brown clusters are not clearly delimited by histology. The statistical differences between these clusters could therefore be related to discrete and probably relevant changes in the peptide/LMW-protein composition, which are undetectable through microscopy alone. In a trial to define the brown and yellow clusters, we performed probabilistic latent semantic analysis (pLSA)⁴¹ with deterministic initialization into the same data set. This statistical technique is a recognized advancement in statistical graphic models, which allows the interpretation of score images and loadings in terms of mass spectral intensities.⁴¹ pLSA results can be interpreted as spatial tissue components and their corresponding mass (m/z) distributions in the tissue component. In this case, pLSA allows a correlation between peptide/protein profiles and a particular region of the tissue. This correlation is particularly interesting for cutaneous leishmaniasis since the infected tissue is composed of preserved and inflamed tissues. There is also a heterogeneous population of defense cells, necrosis, granulomas, amastigotes and preserved tissue.

The estimated number of components to run pLSA analysis was determined in a semi-supervised manner, in which the number of segments was chosen according to the results obtained from histology. We used four components for both infections, referring to four different events that predominate during the infection: (i) preserved tissue, (ii) cellular infiltrates, (iii) necrosis and (iv) granulomas (Fig. 2). MALDI-IMS of the tissue sections was performed in biological triplicate for each species to guarantee the reproducibility of our findings. Fig. S5 and S6 (ESI[†]) show three of the most relevant spectra at specific m/z intervals for *L. amazonensis* and *L. major* from tissue sections obtained from different mice.

Fig. 2 illustrates the distribution of pLSA components at different infection times for *L. amazonensis* and *L. major* through the segmentation map. All four components were color assigned according to the results observed from microscopy. Fig. S4 (ESI[†]) shows details on the pLSA components and the distribution for some relevant spectra at specific m/z intervals. The protein profile for each stage of the infection is also represented by pLSA loadings (Fig. 3 and 4).

For both lesions, the preserved tissue (dark blue) is mainly composed of component 2. In *L. amazonensis* lesions, the inflammatory cellular infiltrates (light blue) are composed of component 4, whereas for *L. major* lesions they are composed of component 1. The yellow/brown regions could not be discriminated through microscopy, since necrosis and granulomas were evenly dispersed over these regions. However, their pLSA loadings are different. The reason why the yellow/brown regions are distinguished might be related to another biological event rather than necrosis or granulomas. The yellow/brown regions are composed of components 1 and 3 for *L. amazonensis* lesions and of components 3 and 4 for *L. major* lesions.

Evaluation of the most relevant pLSA loadings for each stage of infection reveals how the abundance of particular m/z intervals increases or decreases during both infections. The intensity box plot chart (Fig. S7, ESI[†]) represents the intensities of a given m/z interval filtered by the visible regions as a function of different times.

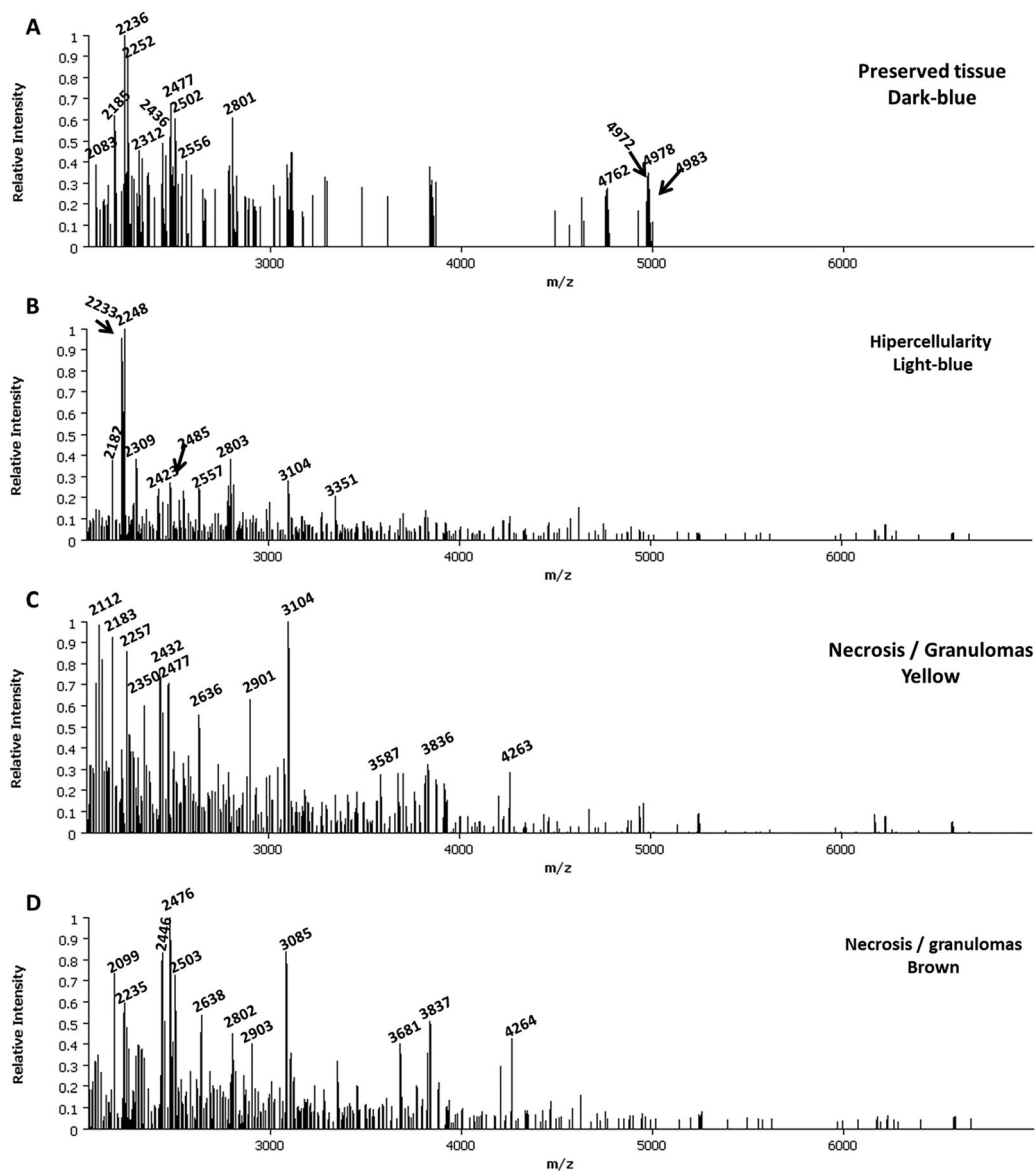


Fig. 3 pLSA loading plots for *L. amazonensis* infection. Each loading plot can be interpreted as mass spectra specific of each segment, which we called preserved tissue, hypercellularity, necrosis and/or granulomas.

The receiver operating characteristic (ROC) is a univariate measure quantifying how well a selected m/z interval discriminates two different states. A perfect discrimination would yield an area under the ROC curve (AUC value) equal to 1. The closer the AUC to 0.5, the less discriminant the m/z interval.⁴² Therefore, m/z intervals greater than 0.75 were considered promising biomarkers. Our findings revealed 62 relevant ions for *L. amazonensis* lesions (Table S1, ESI[†]) and 46 for *L. major* (Table S2, ESI[†]). Similarities between the infections caused by *L. amazonensis* and *L. major* could be observed. A total of 24 m/z intervals were found for both lesions, but the most discriminative ions (AUC > 0.85) for each infection were different (Table 1).

Subsequently, a co-localization step was performed using the SCiLS Lab software by Pearson's correlation analysis that considers only statistically significant correlations.^{42,43} The statistical significance p is defined as $p = 0.05$. Fig. 5 and 6 show some co-localized

ions at different times during the infection for both parasites. It is important to note that generally ions co-localized at a given stage tend to increase or decrease in intensity during the infection, representing molecular differences in disease progression. Differences revealed from our findings need to be further investigated, since it would contribute to resolving unsolved questions about the biology of the parasite and the host response against the infection. Furthermore, the identification of potential biomarker candidates would complement current diagnosis methodologies.

Experimental

Leishmania cultivation

L. amazonensis strain MHOM/BR/67/M2269 and *L. major* strain Friedlin were separately maintained by regular passage in

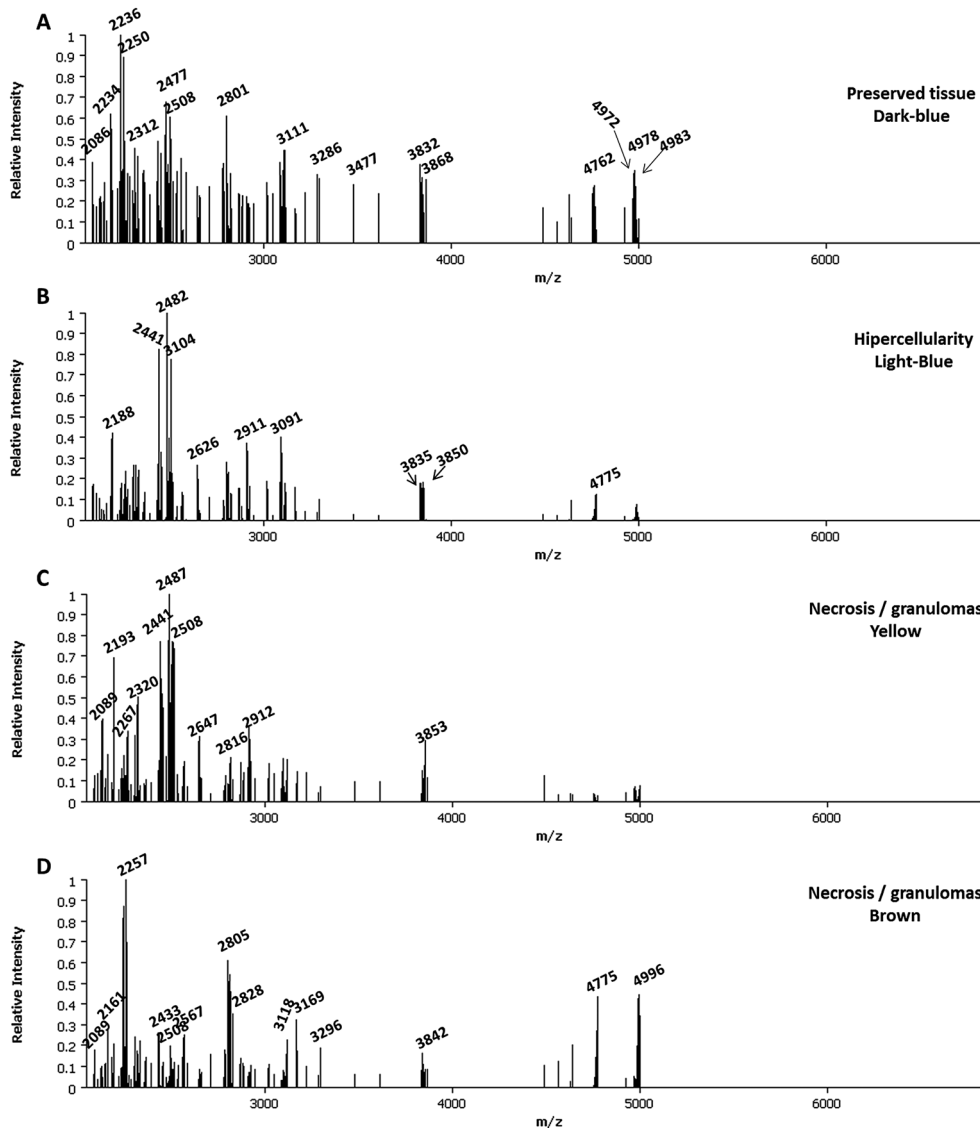


Fig. 4 pLSA loading plots for *L. major* infection. Each loading plot can be interpreted as mass spectra specific of each segment, which we called preserved tissue, hypercellularity, necrosis and/or granulomas.

Table 1 *m/z* intervals (± 10 Da) and AUC values most relevant to *L. amazonensis* and *L. major* infection (AUC > 0.85)

Species	<i>m/z</i>	AUC	Species	<i>m/z</i>	AUC
<i>L. amazonensis</i>	2182	0.986203	<i>L. major</i>	2560	0.896882
<i>L. amazonensis</i>	2234	0.974237	<i>L. major</i>	2804	0.896892
<i>L. amazonensis</i>	2350	0.909499	<i>L. major</i>	2477	0.859242
<i>L. amazonensis</i>	3837	0.892585	<i>L. major</i>	2434	0.851317
<i>L. amazonensis</i>	2248	0.884301	—	—	—
<i>L. amazonensis</i>	2446	0.875408	—	—	—
<i>L. amazonensis</i>	2902	0.875408	—	—	—
<i>L. amazonensis</i>	3837	0.874895	—	—	—
<i>L. amazonensis</i>	2114	0.874895	—	—	—
<i>L. amazonensis</i>	2818	0.874382	—	—	—
<i>L. amazonensis</i>	2474	0.86427	—	—	—
<i>L. amazonensis</i>	2084	0.853084	—	—	—

BALB/c mice.³⁷ Parasites were kept in culture at 26 °C in 5 mL of RPMI medium containing 10% of inactivated fetal bovine

serum at a pH of 7.4. The starter culture contained 10^5 promastigotes in 5 mL of medium and the parasites were used for inoculation in mice.

Animals

The experimental protocols were approved by the Ethical Committee for Animal Research (Protocol number 4140-1) of the Institute of Biology/State University of Campinas. Six-week-old female BALB/c mice, obtained from the Centro de Bioterismo/UNICAMP, were infected in the footpad with 50 μ L containing 5×10^6 promastigotes for each species. The mice were sacrificed by cervical dislocation at different times post-infection (0, 30, 60 and 90 days). At each time (i) three mice infected with *L. amazonensis* and (ii) three mice infected with *L. major* were sacrificed and the footpads were kept frozen at -80 °C until the sectioning time. The negative control was the footpad from an uninfected mouse.

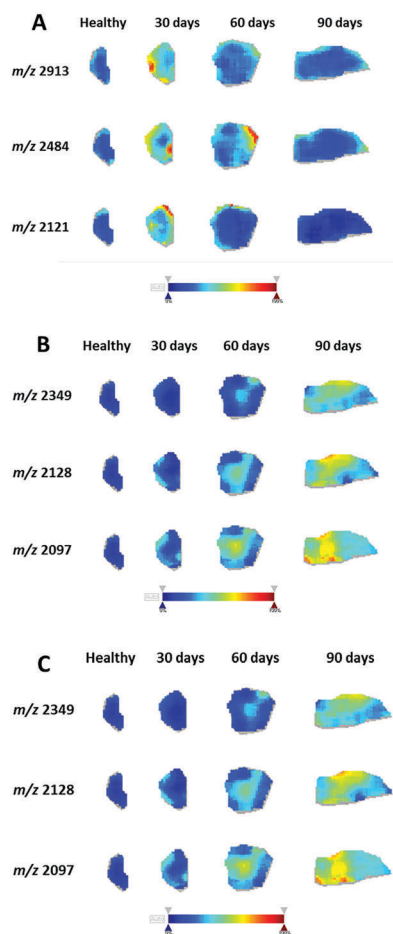


Fig. 5 Co-localized ions at (A) 30 days p.i., (B) 60 days p.i. and (C) 90 days p.i. for *L. amazonensis* infection.

Haematoxylin and eosin staining was used for the histological analysis of the tissue sections, which was performed at each time to confirm the infection.⁴⁴

Sample preparation

A frozen mouse footpad was sliced into a 16 μm tissue sample using a Cryotome (Leica Microsystems, Bannockburn, IL, USA) at $-22\text{ }^{\circ}\text{C}$ and thaw-mounted onto conductive indium-tin-oxide (ITO) coated glass slides (Bruker Daltonics, Bremen, Germany). The subsequent section was analysed through histology using haematoxylin and eosin (H&E) staining to check the adequacy of the frozen material. Tissue slices were air-dried in a desiccator for 30 min. ITO slides were washed following a five-step washing protocol. The washing conditions for the detection of peptides were as follows: 70% ethanol (30 s), 100% ethanol (30 s); ethanol:chloroform:acetic acid solution (6:3:1, % v/v) (2 min), 100% ethanol (30 s), H_2O (30 s), and 100% ethanol (30 s). Then, the samples were dried in a desiccator for 10 minutes prior to the application of the α -cyano-4-hydroxycinnamic acid (CHCA) matrix, which was overlaid onto the tissue sections using a sublimation technique.

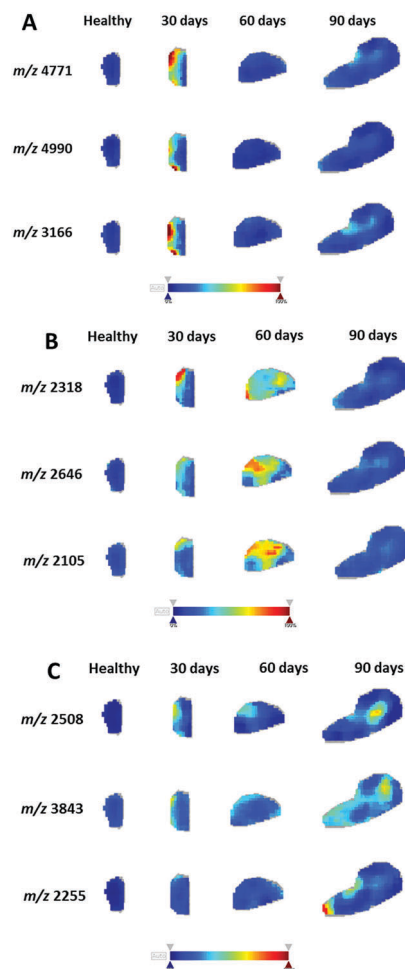


Fig. 6 Co-localized ions at (A) 30 days p.i., (B) 60 days p.i. and (C) 90 days p.i. for *L. major* infection.

Data acquisition

MALDI-IMS analysis was performed in a Bruker Autoflex III, equipped with SmartbeamTM laser technology (Bremem, Germany). Images from the tissue sections were obtained using the FlexControl 3.4 and FlexImaging 4.0 software (Bruker Daltonics, Bremen, Germany). MS data were acquired in linear positive mode in a mass range m/z of 2–10 kDa by 1000 consecutive laser shots in each pixel with a spatial resolution of 150 μm . The laser focus diameter was adjusted to 150 μm .

Data analysis and processing

Data analyses were performed using the SCiLS Lab software (Bruker Daltonics, Bremen Germany). Mass (m/z) shifts were observed in previously analysed samples, thus an interval width of ± 10 Da was chosen. All datasets were pre-processed using baseline subtraction. Data normalization was performed using the total ion count (TIC) method of each spectrum. This method normalizes every spectrum separately by dividing each spectrum intensity by the sum of all its ion peak intensities.³⁹

Subsequently, MS peak picking was performed in the normalized data set reducing the number of ion peaks per

spectrum according to SCiLS default settings. The peak alignment uses the mean spectrum of the complete data set to calculate the alignment.³⁹ Aligned peaks were used to produce the spatial segmentation map with bisecting *k*-means in combination with the correlation distance. Bisecting *k*-means is a top-down clustering method that iteratively divides a set of spectra into two sets that are maximally different according to a metric measure.³⁹ The reduction of the spectrum-to-spectrum variation was accomplished by spatial denoising, which was performed prior to segmentation. All described steps were carried out within the “segmentation pipeline” of the SCiLS Lab software. Probabilistic latent semantic analysis (pLSA), a multivariate analysis, was also performed with 4 components. Furthermore, we used the receiving operating characteristic (ROC curve) and the co-localization tool using the SCiLS Lab software to find relevant *m/z* intervals.

Conclusions

MALDI-IMS of CL has provided for the first time the temporal monitoring of the peptides and LMW proteins that could be directly related – *via* concomitant histological comparisons – to disease progression as well as to the infections caused by two distinct parasites.

Several *m/z* intervals were statistically relevant to disease progression, and according to ROC analysis, cutaneous leishmaniasis is mostly discriminated in *L. amazonensis* infected murine footpads by the ions of *m/z* 2182, 2234, 2350 and 3837, whereas the ions of *m/z* 2560, 2804, 2477 and 2434 were most relevant to *L. major* lesions. MALDI-IMS was therefore shown to be a suitable tool to diagnose CL directly from biopsies of skin lesions as well as to compliment microscopy studies on tissue discrimination by providing biomolecular information for selected surfaces. MALDI-IMS was also shown to contribute to discriminating infections, since statistically relevant differences were not visualized by histology, as shown for instance in Fig. 2 where it could discriminate the yellow and brown clusters assigned by the segmentation map.

Further characterization of the peptides and LMW proteins identified herein as possible biomarkers could reveal their roles in cellular processes regarding *Leishmania* infection. These biomolecules may also function as targets to develop new drugs and diagnosis methodologies.

Conflicts of interest

There are no conflicts to declare.

Acknowledgements

This research was supported by FAPESP (2016/11517-2 and 2015/23767-0).

References

- 1 WHO, Leishmaniasis. WHO, 2016, <http://www.who.int/leishmaniasis/en/>, accessed March 28, 2017.
- 2 WHO, Clinical forms of the leishmaniasis, WHO, 2014, http://www.who.int/leishmaniasis/clinical_forms_leishmaniasis/en/, accessed April 11, 2017.
- 3 C. Cantacessi, F. Dantas-Torres, M. J. Nolan and D. Otranto, *Trends Parasitol.*, 2015, **31**(3), 100–108.
- 4 H. Goto, J. Angelo and L. Lindoso, *Infect. Dis. Clin. North Am.*, 2012, **26**, 293–307.
- 5 H. J. C. de Vries, S. H. Reedijk and H. D. F. H. Schallig, *Am. J. Clin. Dermatol.*, 2015, **16**(2), 99–109.
- 6 D. Rodriguez-Contreras, X. Feng, K. M. Keeney, H. G. A. Bouwer and S. M. Landfear, *Mol. Biochem. Parasitol.*, 2007, **153**(1), 9–18.
- 7 M. A. Vannier-Santos, A. Martiny and W. de Souza, *Curr. Pharm. Des.*, 2002, **8**(4), 297–318.
- 8 M. Podinovskaia and A. Descoteaux, *Future Microbiol.*, 2015, **10**(1), 111–129.
- 9 P. Sampaio, T. Veras, J. Perrone and B. De Menezes, *Int. J. Mol. Sci.*, 2016, **17**(8), 1270.
- 10 B. S. S. Lima, L. C. Fialho, S. F. Pires, W. L. Tafuri and H. M. Andrade, *Vet. Parasitol.*, 2016, **223**, 115–119.
- 11 J. Walker, J. J. Vasquez and M. A. Gomez, *et al.*, *Mol. Biochem. Parasitol.*, 2006, **147**(1), 64–73.
- 12 R. t'Kindt, R. A. Scheltema and A. Jankevics, *et al.*, *PLoS Neglected Trop. Dis.*, 2010, **4**(11), e904.
- 13 A. Kumar, P. Misra, B. Sisodia, A. K. Shasany, S. Sundar and A. Dube, *Parasitol. Int.*, 2015, **64**(4), 36–42.
- 14 R. Reithinger, J.-C. Dujardin, H. Louzir, C. Pirmez, B. Alexander and S. R. Brooker, *Lancet Infect. Dis.*, 2007, **7**(9), 581–596.
- 15 M. H. Wright, D. Paape, E. M. Storck, R. A. Serwa, D. F. Smith and E. W. Tate, *Chem. Biol.*, 2015, **22**(3), 342–354.
- 16 S. Decuyper, M. Vanaerschot and K. Bruncker, *et al.*, *PLoS Neglected Trop. Dis.*, 2012, **6**(2), e1514.
- 17 M. Ehrmann, F. Kaschani and M. Kaiser, *Chem. Biol.*, 2015, **22**(3), 309–310.
- 18 A. L. Bodley and T. A. Shapiro, *Proc. Natl. Acad. Sci. U. S. A.*, 1995, **92**(9), 3726–3730.
- 19 R. t'Kindt, R. A. Scheltema and A. Jankevics, *et al.*, *PLoS Neglected Trop. Dis.*, 2010, **4**(11), e904.
- 20 G. D. Westrop, R. A. M. Williams and L. Wang, *et al.*, *PLoS One*, 2015, **10**(9), e0136891.
- 21 J. P. B. Menezes, T. F. Almeida and A. L. O. A. Petersen, *et al.*, *Microbes Infect.*, 2013, **15**(8–9), 579–591.
- 22 D. de S. Moreira, P. Pescher, C. Laurent, P. Lenormand, G. F. Späth and S. M. F. Murta, *Proteomics*, 2015, **15**(17), 2999–3019.
- 23 I. Serafin-Higuera, O. L. Garibay-Cerdenares and B. Illades-Aguar, *et al.*, *Proteome Sci.*, 2016, **14**(1), 10.
- 24 H. A. Ebhardt, A. Root, C. Sander and R. Aebersold, *Proteomics*, 2015, **15**, 3193–3208, DOI: 10.1002/pmic.201500004.
- 25 L. Eberlin, D. Ifa, C. Wu, R. Cooks and M. Graha, *Angew. Chem., Int. Ed.*, 2010, **49**(5), 873–876.
- 26 M. M. Gessel, J. L. Norris and R. M. Caprioli, *J. Proteomics*, 2014, **107**, 71–82.

- 27 L. S. Eberlin, I. Norton and A. L. Dill, *et al.*, *Cancer Res.*, 2012, **72**(3), 645–654.
- 28 B. Balluff, S. Rauser, M. P. Ebert, J. T. Siveke, H. Höfler and A. Walch, *Gastroenterology*, 2012, **143**(3), 544.
- 29 B. Cillero-Pastor and R. M. A. Heeren, *J. Proteome Res.*, 2014, **13**(2), 325–335.
- 30 X. Xie, Y. Jiang and Y. Yuan, *et al.*, *Oncotarget*, 2016, **7**(37), 59987–60004.
- 31 C. Zhang, G. Arentz and L. Winderbaum, *et al.*, *Int. J. Mol. Sci.*, 2016, **17**(7), 1088.
- 32 M. L. Reyzer, R. L. Caldwell and T. C. Dugger, *et al.*, *Cancer Res.*, 2004, **64**(24), 9093–9100.
- 33 M. Roesch-Ely, M. Nees and S. Karsai, *et al.*, *Oncogene*, 2007, **26**(1), 54–64.
- 34 N. Poté, T. Alexandrov and J. Le Faouder, *et al.*, *Hepatology*, 2013, **58**(3), 983–994.
- 35 B. F. Cravatt, G. M. Simon and J. R. Yates III, *Nature*, 2007, **450**(7172), 991–1000.
- 36 M. A. Lynn, A. K. Marr and W. R. McMaster, *J. Proteomics*, 2013, **82**, 179–192.
- 37 D. F. de O. Rocha, C. F. Jaeger and F. Negrão, *et al.*, *Mol. BioSyst.*, 2017, DOI: 10.1039/c7mb00306d.
- 38 T. Alexandrov, S. Meding and D. Trede, *et al.*, *J. Proteomics*, 2011, **75**(1), 237–245.
- 39 T. Alexandrov, M. Becker and S.-O. Deininger, *et al.*, *J. Proteome Res.*, 2010, **9**(12), 6535–6546.
- 40 D. Trede, S. Schiffler, M. Becker, *et al.*, SCiLS Lab 2D: Spatial segmentation with edge-preserving image denoising. <http://scils.de/wp-content/uploads/2016/05/SCiLS-Application-note3.pdf>, accessed May 11, 2017.
- 41 M. Hanselmann, M. Kirchner and B. Y. Renard, *et al.*, *Anal. Chem.*, 2008, **80**(24), 9649–9658.
- 42 T. Alexandrov, MALDI imaging mass spectrometry: statistical data analysis and current computational challenges, *BMC Bioinf.*, 2012, S11, DOI: 10.1186/1471-2105-13-S16-S11.
- 43 L. A. McDonnell, A. van Remoortere, R. J. M. van Zeijl and A. M. Deelder, *J. Proteome Res.*, 2008, **7**(8), 3619–3627.
- 44 R. D. Cardiff, C. H. Miller and R. J. Munn, *Cold Spring Harbor Protoc.*, 2014, **2014**(6), 655–658.